The Astrophysical Journal, 837:81 (10pp), 2017 March 1 https://doi.org/10.3847/1538-4357/aa5e52

The Optical/UV Excess of X-Ray-dim Isolated Neutron Stars. I. Bremsstrahlung Emission from a Strangeon Star Atmosphere

Weiyang Wang[1,2,3], Jiguang Lu[1], Hao Tong[4], Mingyu Ge[5], Zhaosheng Li[6], Yunpeng Men[1], and Renxin Xu[1,7]
[1] School of Physics and State Key Laboratory of Nuclear Physics and Technology, Peking University, Beijing 100871, China; r.x.xu@pku.edu.cn
[2] Key Laboratory of Computational Astrophysics, National Astronomical Observatories, Chinese Academy of Sciences, Beijing 100012, China
[3] University of Chinese Academy of Sciences, Beijing 100049, China
[4] Xinjiang Astronomical Observatory, Chinese Academy of Sciences, Urumqi 830011, China
[5] Key Laboratory for Particle Astrophysics, Institute of High Energy Physics, Chinese Academy of Sciences, Beijing 100049, China
[6] Department of Physics, Xiangtan University, Xiangtan 411105, China
[7] Kavli Institute for Astronomy and Astrophysics, Peking University, Beijing 100871, China (FAST Fellow distinguished)
Received 2016 March 27; revised 2017 January 28; accepted 2017 January 30; published 2017 March 6

Abstract

X-ray-dim isolated neutron stars (XDINSs) are characterized by Planckian spectra in X-ray bands, but show optical/ultraviolet (UV) excesses: the factors by which the measured photometry exceeds those extrapolated from X-ray spectra. To solve this problem, a radiative model of bremsstrahlung emission from a plasma atmosphere is established in the regime of a strangeon star. A strangeon star atmosphere could simply be regarded as the upper layer of a normal neutron star. This plasma atmosphere, formed and maintained by the interstellar-medium-accreted matter due to the so-called strangeness barrier, is supposed to be of two temperatures. All seven XDINS spectra could be well fitted by the radiative model, from optical/UV to X-ray bands. The fitted radiation radii of XDINSs are from 7 to 13 km, while the modeled electron temperatures are between 50 and 250 eV, except RX J0806.4–4123, with a radiation radius of ∼3.5 km, indicating that this source could be a low-mass strangeon star candidate. This strangeon star model could further be tested by soft X-ray polarimetry, such as the Lightweight Asymmetry and Magnetism Probe, which is expected to be operational on China's space station around 2020.

Key words: elementary particles – pulsars: general – radiation mechanisms: general – stars: atmospheres – stars: neutron

1. Introduction

The *ROSAT* all-sky observations (Voges et al. 1996) led to the discovery of seven nearby isolated neutron stars (NSs; hereafter "NS" refers to all kinds of pulsar-like compact objects) that predominantly show thermal emission. These seven isolated NSs are then called X-ray-dim isolated neutron stars (XDINSs), characterized by their Planck-like spectra in X-ray bands and their location in the upper right of the pulsar P–$\dot{P}$ diagram (see, e.g., Tong 2016). They are peculiar objects for us to study the NS surface (atmosphere), as well as the equation of state at supranuclear density.

RX J1856.5–3754 (J1856 hereafter as other sources) is the brightest source among all XDINSs and has a Planck-like featureless spectrum (Burwitz et al. 2001) without a significant high-energy tail. Besides the spectrum of J1856, those of other XDINSs can also be described as pure blackbodies (with a broad absorption feature at 271 eV [Haberl et al. 2004] for RX J0720.4–3125, while at 400 eV [van Kerkwijk et al. 2004] for RX J1605.3+3249). Compared with the optical bands, the extrapolated X-ray spectrum of J1856 is reduced by a factor of ∼7 (Burwitz et al. 2003). This measured photometry exceeds those extrapolated from X-ray spectra, which is referred to as the optical/ultraviolet(UV) puzzle. Up until this point, for all XDINSs, optical counterparts have been searched in deep optical observations, leading to the fact that most sources have optical excesses between 5 and 12 (Kaplan et al. 2011). RX J1308.6+2127 has an excess of ∼3.8 at 1500 Å. The optical and UV fluxes of RX J2143.0+0654 exceed the X-ray extrapolation by a factor of more than 50 at 5000 Å with a flux $F_\nu \propto \nu^\beta$ ($\beta \sim 0.5$; Kaplan et al. 2011).

More than a few efforts have been made to understand the optical/UV excess of XDINSs. For instance, in a two-component blackbody model of J1856, the temperature of the hot component is $kT_{\rm X}^{\infty} \sim 63.5$ eV with radiation radius $R_{\rm X}^{\infty} \sim 4.4(d/120\ {\rm pc})$km, while that of the cold part is $kT_{\rm opt} < 33$ eV ($R_{\rm opt}^{\infty} > 17(d/120\ {\rm pc})$km; Burwitz et al. 2003; Trümper et al. 2004). The radiation radius of the hot component may be smaller than that of a typical NS, while the radius of the cold one is bigger (van Kerkwijk & Kaplan 2007). Alternatively, the emission is suggested to come from the condensed matter surface (Lai 2001; Turolla et al. 2004).

We are interpreting here that the emission comes from a strangeon star plasma atmosphere. "Strangeon," formerly known as "strange quark-cluster" (Xu 2003), is actually coined by combining "strange nucleon." However, a strangeon star is different from a strange quark star even though both of them are usually mentioned by the name of the strange star for their strangeness. In fact, J1856, with the featureless spectrum and a small apparent radius (∼5 km), might be a strange quark star (Drake et al. 2002; Xu 2002). However, in this paper, we are considering and modeling XDINS spectra assuming that they are strangeon stars, which are condensed matter objects of strangeons (i.e., three-flavored quark-clusters). It is worth noting that strange quark stars and strangeon stars (quarks are free in the former but localized in the latter) behave very differently in astrophysics (see, e.g., Xu & Guo 2017, p. 119, for a review). The plasma atmosphere of a strangeon star is made up of the ionized normal matter and is supposed to be of two temperatures (Xu 2014). The bremsstrahlung model presented here is devoted to fitting the spectra of seven XDINSs from X-ray to optical/UV bands and concludes with

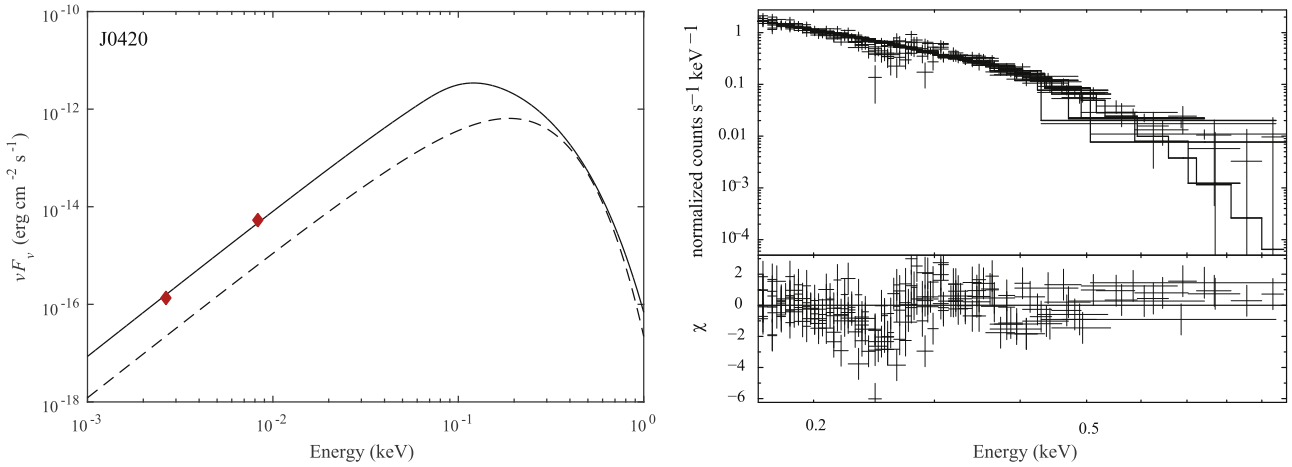

Figure 1. Bremsstrahlung curve (left, solid line) and X-ray data fitting (right) of J0420 are shown. The solid curve (with parameters listed in Table 1 for J0420) plotted in the left panel is calculated in the bremsstrahlung radiation model of a plasma atmosphere above a strangeon star. By comparison, a dashed line representing the pure blackbody model extrapolated from its X-ray spectrum is also drawn. The red diamonds represent optical observations from the *HST* photometry (Kaplan et al. 2011). The extracted spectra are binned with 50 counts per bin in each observation at least. The X-ray data (0.21–0.28 keV ignored) are fitted by the bremsstrahlung model. The spectrum presents a broad absorption line around 0.25 keV, with a width of $\sigma = 0.04$ keV.

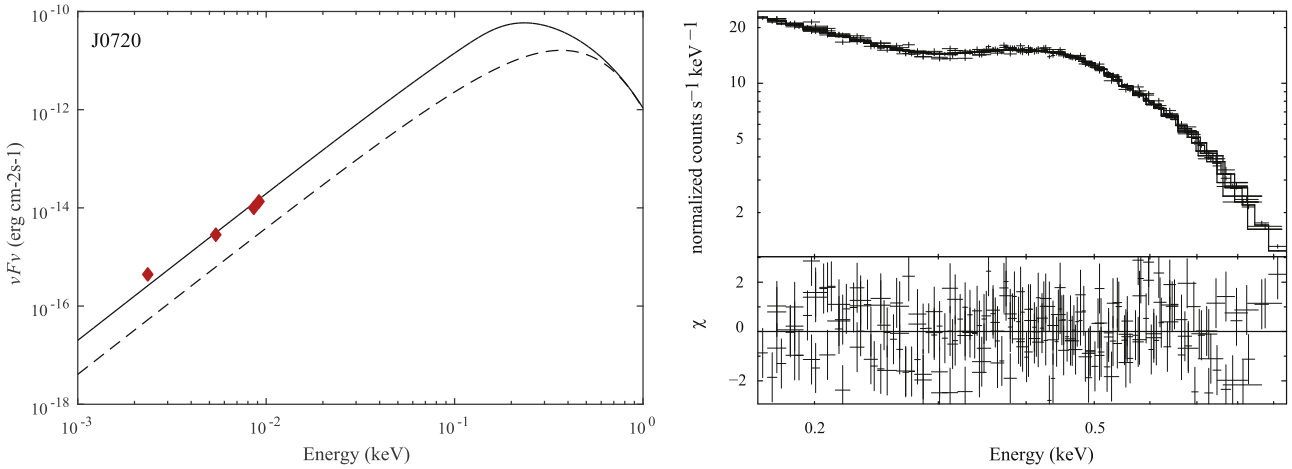

Figure 2. Same as in Figure 1, but for J0720. The extracted spectra are binned with 1000 counts per bin in each observation at least. The X-ray data are fitted by the bremsstrahlung plus a power law ($F = K\left(\frac{h\nu}{1\,\mathrm{keV}}\right)^{-\beta}$, where $\beta = 6.5 \pm 0.4$ and $K = (6.8 \pm 4.4) \times 10^{-6}$ counts s^{-1} keV^{-1}), with the same hydrogen column density.

reliable radiation radii ($\sim$10 km) and electron temperatures ($\sim$100 eV).

In Section 2, the process of bremsstrahlung in a strangeon star plasma atmosphere and the emissivity are presented. In Section 3, we fit the spectra of seven XDINSs. Finally, we provide our discussions and a summary in Sections 4 and 5, respectively.

2. Bremsstrahlung Radiation in a Strangeon Star Atmosphere

In this section, we interpret the formation of the atmosphere and calculate its emission, with a brief introduction to strangeon stars at first.

The state of dense baryonic matter compressed during a supernova is not yet well understood because of the non-perturbative nature of the fundamental strong interaction, but it is popularly speculated that compact stars are composed of nucleons (this kind of matter should be actually neutron-rich because of the weak interaction, and we thus usually call them NSs). However, these compact stars are alternatively proposed to be strangeon stars (Xu 2003). The constituent quarks in a strangeon are of three flavors (u, d, and s) rather than of two flavors for normal nucleons. Certainly, the fundamental weak interaction does play an essential role in converting normal two-flavor matter (i.e., nucleons) into three-flavor matter (i.e., strangeons) during an accretion phase. The weak conversion, however, is not easy and could be successful only after frequent collisions (order of $\gg$1), similar to the famous *pp*-reaction with flavor change. Therefore, we introduce the term "strangeness barrier" to describe this kind of difficulty (Xu 2014).

Different manifestations could be understood in the strangeon star model, including very stiff equations of state (Lai & Xu 2009), two types of pulsar glitches (Zhou et al. 2014), X-ray flares and bursts of magnetar candidates (Xu et al. 2006), and even the central-engine plateau of gamma-ray bursts (Dai et al. 2010). In addition, the strangeness barrier could also be meaningful to understanding Type I X-ray bursters, as well as constraining their masses and radii (Li et al. 2015). Despite these, we try to solve the optical/UV excess puzzle with a

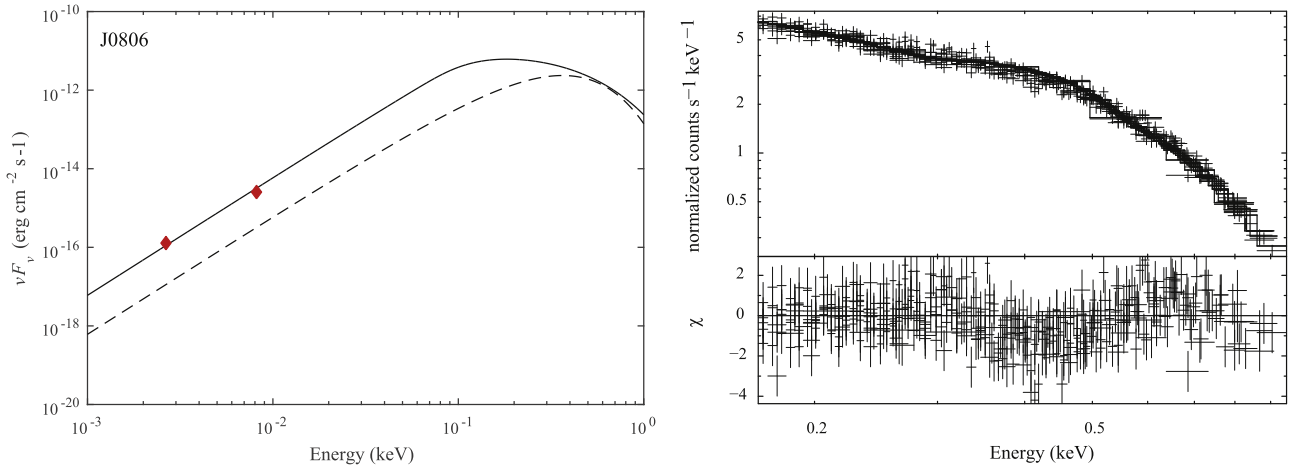

Figure 3. Same as in Figure 1, but for J0806. The extracted spectra are binned with 50 counts per bin in each observation at least. The X-ray data (0.36–0.46 keV ignored) are fitted by the bremsstrahlung model. The spectrum presents a broad absorption line around 0.41 keV ($\sigma = 0.05$ keV) .

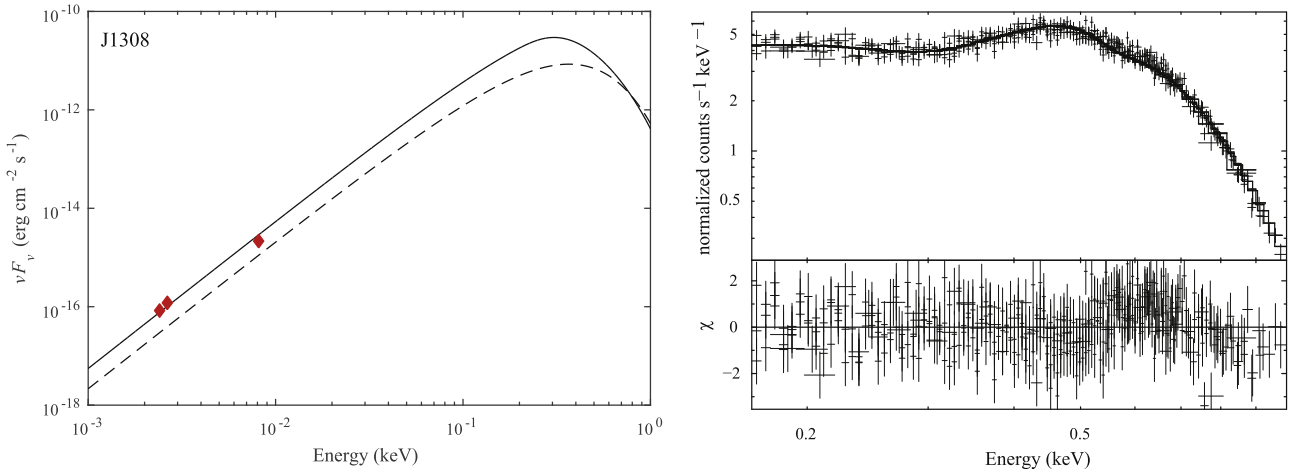

Figure 4. Same as in Figure 1, but for J1308. The extracted spectra are binned with 100 counts per bin in each observation at least. The X-ray data are fitted by the bremsstrahlung plus a Gaussian function, which indicates an absorption line around 0.23 keV ($\sigma = 0.08$ keV).

strangeon star atmosphere, which is a direct consequence of the barrier.

2.1. Formation of the Plasma Atmosphere of a Strangeon Star

The interstellar medium (ISM) could be attracted onto an isolated strangeon star through gravitational force, but the magnetosphere represents an obstacle for the flow (Toropina et al. 2001). We assume that the spatial velocity $\boldsymbol{v}_s$ of the isolated NS is much greater than the sound velocity $\boldsymbol{c}_s$ in the ISM. According to the classical accretion proposed by Bondi–Hoyle–Littleton (Bondi 1952), the ISM is gravitationally captured by an NS inside the Bondi radius,

$$R_B = \frac{2GM}{v_s^2}, \tag{1}$$

where G is the gravitational constant and M is the mass of the star, which is typically considered to be $1.4\,M_\odot$. ISM accretion is proposed to make isolated NSs shine with weak soft X-ray luminosity (e.g., Treves et al. 2000). For the X-ray luminosity of XDINSs, $\sim 10^{31}$–10^{32} erg s^{-1} (Kaplan & van Kerkwijk 2009), one could estimate an accretion rate of $\dot{M}_X \sim 10^{10}$–10^{11} g s^{-1}, which should equal approximately the accretion rate $\dot{M}_B$ proposed by Bondi (1952). The Bondi accretion rate is formulated as

$$\dot{M}_B = \rho_\infty v_s \pi R_B^2, \tag{2}$$

where ρ_∞ is the ISM matter density (below we assume the density to be the typical value of $\sim 10^{-24}$ g cm^{-3}). From Equations (1) and (2), the spatial velocity ($\sim 10^6$–10^7 cm s^{-1}) and the Bondi radius are calculated, $R_B \sim 10^{12}$ cm. In the case of a surface magnetic field of $\lesssim 10^{12}$ G, the Alfvén radius $R_A \lesssim R_B$. For Alfvén radius $R_A \sim R_B$, the star captures matter gravitationally from the accretion disk. In the regime that $R_A \sim R_B$, part of the ISM accumulates around the NS, but most of it is deflected by the magnetic field of the star and flies away (Toropina et al. 2001).

Accretion may make the central star be covered by a corona/atmosphere (in the case of a low accretion rate) or even a crust (high accretion rate, in binary), due to its strangeness barrier (Xu 2014). It is worth noting that the Coulomb barrier

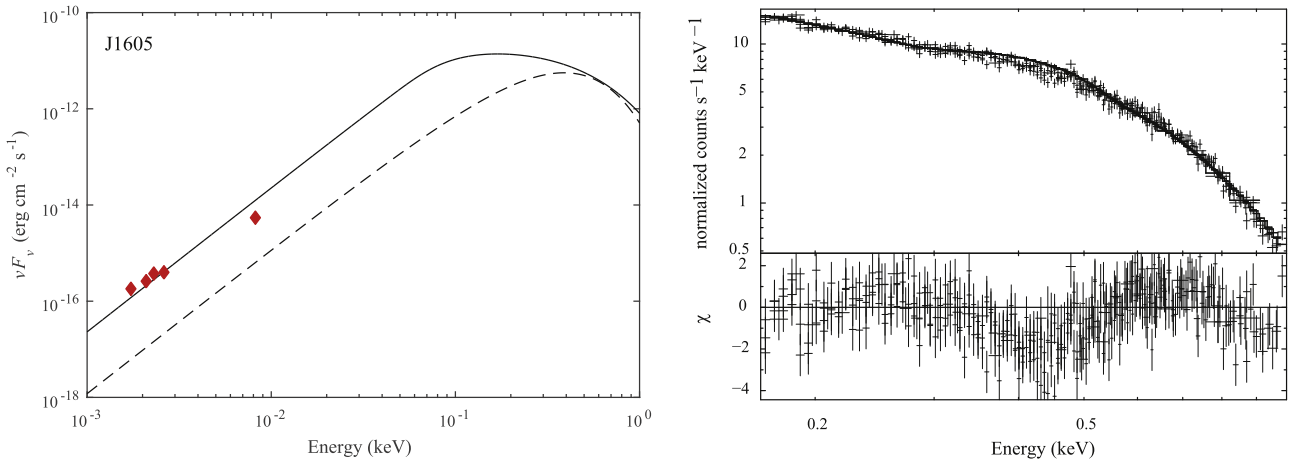

Figure 5. Same as in Figure 1, but for J1605. The extracted spectra are binned with 500 counts per bin in each observation at least. The X-ray data (0.37–0.5 keV ignored) are fitted by the bremsstrahlung model. The spectrum presents a broad absorption line around 0.44 keV ($\sigma = 0.06$ keV).

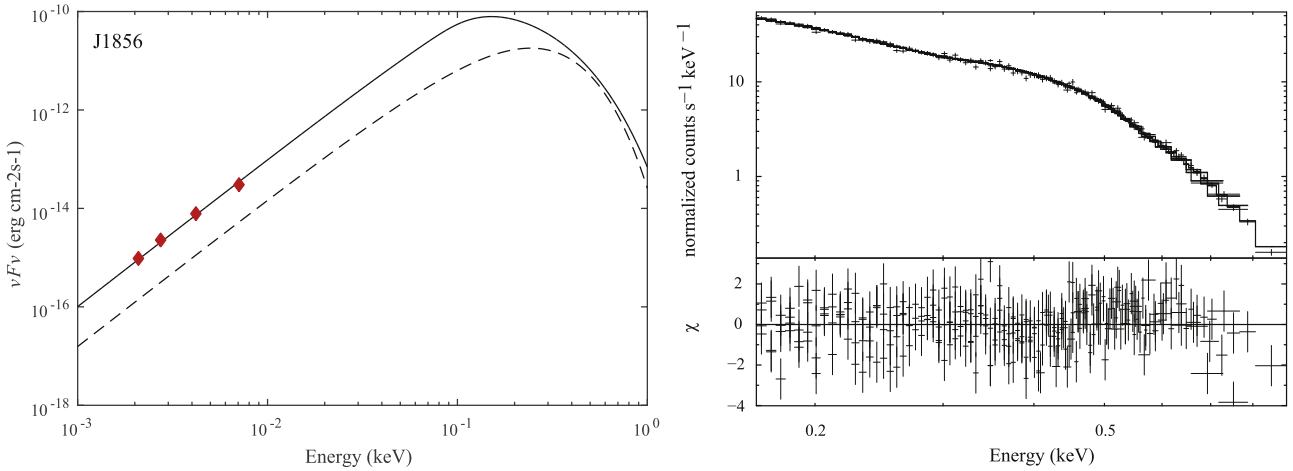

Figure 6. Same as in Figure 1, but for J1856. The extracted spectra are binned with 1000 counts per bin in each observation at least. The X-ray data are fitted by the bremsstrahlung plus a Gaussian function, which indicates an absorption line around 0.21 keV ($\sigma = 0.02$ keV).

of strangeon stars cannot effectively prevent ISM-accreted matter from penetrating into the star (Xu 2002), as the kinetic energy (10–100 MeV) is comparable to or even higher than the Coulomb barrier energy (∼10 MeV). Nonetheless, most of the falling nonstrange normal nuclei would be bounced back along the magnetic field lines because nonstrange matter cannot become part of strange matter unless it is converted to strangeons via weak interaction (i.e., *u/d* changed to *s* quarks). With the typical timescale for weak interaction $\tau_{\rm weak} \sim 10^{-7}$ s and the speed of ion is in the range of $v_{\rm i} \sim (10^{-3} - 10^{-1})c$, where c is the speed of light, the probability of ions that would successfully change flavor to strangeon could be of the order of $\sim 10^{-15}$ to 10^{-13}. Also, by analogy with spontaneous emission from an atom via electromagnetic interactions, with the inclusion of the energy dependence (E^3; see, e.g., van Driel et al. 2005, for a test of the E^3 dependence) of the rate, the probability of weak interactions would be enhanced by a factor of 10^3–10^5 if a value of energy ∼30–100 MeV were released per baryon during the phase conversion. Actually, the probability of normal matter being converted into strange-cluster matter could be enhanced if the strong interaction is included (e.g., $p + \pi^- \leftrightarrow \Lambda^0 + K^0$, but details of the calculation on the strange-cluster matter surface will be addressed in the future). In summary, there is not enough time to convert an up/down quark inside a nucleus into a strange quark during the collision between a nucleus and strangeon, and the conversion rate is then comparably low for accreted nuclei. Certainly, there is still a small portion of nonstrange normal nuclei that could permeate into the star's interior, i.e., penetrating the strangeness barrier.

This barrier could be helpful to produce a corona, which would be essential for understanding the puzzling observations of symbiotic X-ray system 4U 1700+24 (Xu 2014). A corona/atmosphere loses energy continuously by radiation. Meanwhile, through collision, newly accreted nuclei provide energy for the corona/atmosphere that keeps it at a quasi-constant temperature.

Noteworthily, the plasma atmosphere (corona) is of two temperatures. In fact, an electron loses its energy faster than an ion by radiation because, in bremsstrahlung processes, the energy-losing rate of particles is inversely proportional to the square of the particle mass (see Equation (6)), and the mass of

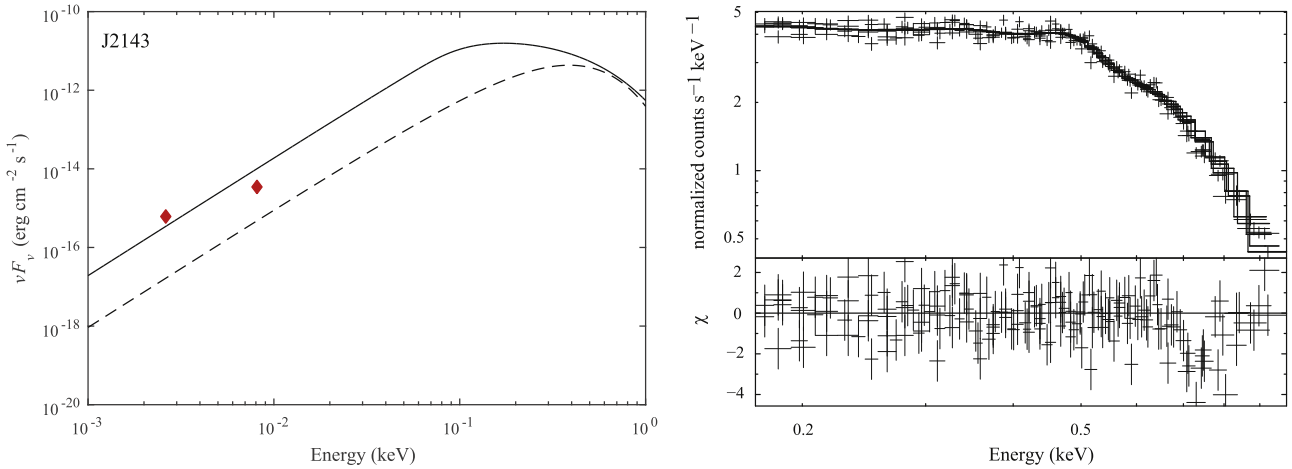

Figure 7. Same as in Figure 1, but for J2143. The extracted spectra are binned with 150 counts per bin in each observation at least. The X-ray data (0.68–0.78 keV ignored) are fitted by the bremsstrahlung plus a Gaussian function. The spectrum of J2143 might present absorption lines around 0.23 keV ($\sigma = 0.12$ keV) and 0.73 keV ($\sigma = 0.05$ keV).

Table 1
Parameters Obtained from X-Ray Spectral Fitting

Source RX	kT_e (eV)	R_{opt}^{∞} (km)	y ($\times 10^{42}$ cm^{-6} keV)	Absorption (keV)	N_H ($\times 10^{20}$ cm^{-2})	d (pc)	Total Counts	χ^2/dof
J0420.0−5022	71.6 ± 2.5	9.3 ± 0.3	1.49 ± 0.25	0.25	1.60 ± 0.47	345	11806	1.15/131
J0720.4−3125[a]	152.1 ± 2.0	10.2 ± 0.1	15.32 ± 1.71	…	1.65 ± 0.39	360	582069	1.41/218
J0806.4−4123	195.2 ± 2.4	3.5 ± 0.1	1.15 ± 0.05	0.41	2.30 ± 0.07	250	79908	1.11/321
J1308.6+2127	106.3 ± 6.1	9.3 ± 0.1	248.36 ± 143.57	0.23	8.59 ± 0.99	500	64217	1.09/405
J1605.3+3249	217.0 ± 2.2	9.9 ± 0.1	2.33 ± 0.07	0.44	1.94 ± 0.07	390	113076	1.15/286
J1856.5−3754	97.5 ± 0.4	12.8 ± 0.1	4.61 ± 0.13	0.21	3.01 ± 0.06	160	733000	1.17/298
J2143.0+0654	136.1 ± 10.0	12.6 ± 0.9	21.48 ± 10.62	0.23 and 0.73	11.94 ± 3.04	430	88466	1.05/158

Notes. Columns (1)–(9) are source name ("Source RX"), temperature of electrons ("kT_e"), radius of stars ("R_{opt}^{∞}"), parameter y, absorption lines, neutral hydrogen column density ("N_H"), distance ("d"), total counts, and χ^2/degree of freedom. Errors on the spectral model parameters are derived for a 90% confidence level. The distances are from Kaplan & van Kerkwijk (2009).
[a] A power-law component with index about 6.5 is also introduced during the fitting of J0720.

ions is much greater than that of electrons. This could make the plasma atmosphere of two temperatures, and the temperature of ions T_i should be much higher than that of electrons T_e ($T_i \gtrsim 0.1$ keV but much lower than 100 MeV). The observed thermal X-ray is mainly related to the temperature of electrons (Xu 2014).

As suggested previously for strange quark stars, the total mass of the plasma atmosphere ΔM is estimated to be $\sim 10^{-24}$ to $10^{-23}\,M_\odot$ (Usov 1997) with the X-ray timescale $\tau_X \sim 0.01$–1 s due to the luminosity of XDINSs. Also, the scale height of the plasma atmosphere H could be approximately described as

$$kT_i \simeq \frac{GMm_i}{R^2}H = \frac{4\pi}{3}Gm_iRH\rho, \quad (3)$$

where m_i is the mass of ions, ρ is the mass density, and R is the radius of the star. As we assume ρ to be 1.5 times the atomic nucleus density in the following calculation, we then have 1 cm $\lesssim H \ll R$. The bounced ions collide with the star many times in plasma atmosphere, and the frequency of the collision is $f_c \simeq 2v_i/H \sim 10^5$–$10^8$ s^{-1}. If there is a stable equilibrium between accretion and permeation for these falling ions, the probability of ions that would permeate into the star $\eta \simeq \dot{M}_X/(f_c\Delta M) \sim 10^{-8}$.

The density of the plasma atmosphere is extremely low, which is different from Zavlin et al. (1996), due to the low accretion rate. The atmosphere that we are focusing on could be considered simply as the upper layer of the atmosphere of normal NSs, but with two temperatures. With the increase of height, the value of the Coulomb interaction decreases very quickly (Alcock et al. 1986), so we only consider the gravity while calculating the distribution of ions and electrons in the plasma atmosphere. In the following, it is assumed that the plasma atmosphere is spherically symmetric and is of thermodynamic equilibrium. According to the Boltzmann distribution and the condition of electrical neutrality, the number density of ions n_i and that of electrons n_e follow

$$n_e = n_i = n_{i0}e^{-\frac{m_igz}{kT_i}}, \quad (4)$$

where n_{i0} and z are the number density of ions in the bottom of the atmosphere and the height above the star's surface, respectively, and g is the gravitational acceleration above the surface of a strangeon star. For a strangeon star with mass around $\sim 1\,M_\odot$, one could approximate

$$g = \frac{GM}{R^2} = \frac{4\pi GR\rho}{3} = 0.0279 \times \frac{\rho}{\mathrm{g\,cm^{-3}}}\frac{R}{\mathrm{km}}\ \mathrm{cm\,s^{-2}}. \quad (5)$$

2.2. Bremsstrahlung from the Plasma Atmosphere

We propose that the observed thermal X-ray is the result of the bremsstrahlung radiation from the plasma atmosphere. The bremsstrahlung emission is mainly generated by collisions of ions and electrons in the plasma atmosphere. When ions scatter high-speed electrons with small angles, the emission coefficient of a single-speed electron can be described as (Rybicki & Lightman 1979)

$$j = \frac{32\pi^2 Z^2 e^6 n_i n_e}{3m_e^2 v c^3} \ln \frac{b_{max}}{b_{min}}, \quad (6)$$

where b is the impact parameter, e is the elementary charge, m_e is the mass of electrons, v is the speed of electrons, and b_{max} could be simply taken as v/ω. We assume that ions are mainly composed of protons ($Z \sim 1$) in the following calculations. Due to the temperature of electrons kT_e is higher than the Rydberg energy of the hydrogen atom, b_{min} would be described by the uncertainty relation that is (Rybicki & Lightman 1979)

$$b_{min} = \frac{h}{m_e v}, \quad (7)$$

with h the Planck constant.

In a plasma atmosphere, electrons and ions could be approximated in two thermal equilibrium states with different temperatures. We can average the emission coefficient of a single-speed electron over the 3D Maxwell velocity distribution. In the average integration, the cutoff in the lower limit over electron velocity should be $v_{min} = \sqrt{2h\nu/m_e}$, where $h\nu$ is the energy of a photon and v_{min} is the minimum speed of an electron that can excite a photon. Then the thermal statistical emission coefficient is (Rybicki & Lightman 1979)

$$\begin{aligned} j_\nu &= \frac{32\pi^2 e^6}{3m_e^{1.5} c^3} \sqrt{\frac{2}{h\nu}} n_{i0}^2 e^{\frac{-2m_i gz}{kT_i}} e^{-\frac{h\nu}{kT_e}} \\ &= 6.16 \times 10^{-41} \frac{n_{i0}^2 e^{-\frac{h\nu}{kT_e} - \frac{2m_i gz}{kT_i}}}{\sqrt{(h\nu)_{keV}}} \text{ erg Hz}^{-1} \text{ s}^{-1} \text{ cm}^{-3}. \end{aligned} \quad (8)$$

According to Kirchhoff's law, the thermal free–free absorption coefficient

$$\begin{aligned} \alpha_\nu = \frac{j_\nu}{B_\nu} &= \frac{16\pi\sqrt{2} h^2 n_{i0}^2 e^6 e^{\frac{-2m_i gz}{kT_i}}}{3m_e^{1.5} c (h\nu)^{3.5}} (1 - e^{-\frac{h\nu}{kT_e}}) \\ &= 9.41 \times 10^{-47} \frac{n_{i0}^2 e^{\frac{-2m_i gz}{kT_i}}}{(h\nu)_{keV}^{3.5}} (1 - e^{-\frac{h\nu}{kT_e}}) \text{cm}^{-1}, \end{aligned} \quad (9)$$

where B_ν is the Planck function. The monochromatic radiation intensity I_ν obeys

$$\frac{dI_\nu}{ds} = j_\nu - \alpha_\nu I_\nu, \quad (10)$$

where $s = z/\cos\varphi$ and φ is the zenith angle, with the sight line considered as the pole axis. The radiation from a bare strange quark star is far less than that of the atmosphere (Xu 2002; Zakharov 2011) that shows the boundary condition of Equation (10) $\{z = 0, I_\nu = 0\}$. Under this circumstance, the solution of Equation (10) presents the monochromatic radiation intensity,

$$I_\nu = B_\nu (1 - e^{-\tau(s,\nu,\varphi)}), \quad (11)$$

where $\tau(s, \nu, \varphi)$ is the optical depth,

$$\tau(s, \nu, \varphi) = \frac{e^{\frac{2m_i gs}{kT_i}} - 1}{\frac{2m_i g}{kT_i} \cos\varphi} \alpha_\nu. \quad (12)$$

The radiation radius R_{opt}^{∞} is approximately the radius R when H is much less than R. We can also have a geometrical relationship,

$$\frac{\sin\theta}{R} \simeq \frac{\sin\varphi}{d}, \quad (13)$$

where θ is the angle between the radiation direction and sight line, and d is the distance from the source. Without the temperature gradient of electrons in the plasma atmosphere considered, the flux of the radiation could be described as

$$F_\nu(s) = \int I_\nu \cos\theta d\Omega \simeq \pi B_\nu (1 - e^{-\tau(s,\nu)}), \quad (14)$$

where $d\Omega$ is the solid angle. The observed radiation should be gravitationally redshifted, i.e.,

$$F_\nu^{\infty} \simeq \pi \left(\frac{R_{opt}^{\infty}}{d}\right)^2 B_\nu (1 - e^{-\tau_\infty(\nu)}), \quad (15)$$

where $\tau_\infty(\nu)$ is the observed optical depth at the far field,

$$\begin{aligned} \tau_\infty(\nu) &= \frac{8\pi\sqrt{2} h^2 n_{i0}^2 e^6 kT_i}{3m_e^{1.5} (h\nu)^{3.5} m_i g c} (1 - e^{-\frac{h\nu}{kT_e}}) \\ &= 3.92 \times 10^{-45} \frac{n_{i0}^2 (kT_i)_{keV}}{(h\nu)_{keV}^{3.5} R_{km}} (1 - e^{-\frac{h\nu}{kT_e}}). \end{aligned} \quad (16)$$

It is assumed that $n_{i0}^2 (kT_i)_{keV} \sim 10^{42}$ cm^{-6} keV, and from Equations (15) and (16) we can calculate and find that the emission is optically thick at optical/UV bands, resembling a Rayleigh–Jeans regime, while it is optically thin at X-ray bands. Thus, the data of these bands can be fitted separately.

3. Data Reduction and Fitting

The raw spectrum data are processed with the *XMM-Newton* science analysis package, called Science Analysis System v14.0. All X-ray data are collected by the European Photon Imaging Camera (EPIC)-pn camera, while the two EPIC-MOS detectors are not considered in our analysis because the MOS effective area at soft X-ray energies is much smaller than that of the pn, and the MOS cameras are known to be less stable for a long-term study (Read et al. 2006). The right ascension, declination, observation start date, observation end date, exposure time, and counts of XDINSs for each observation are reported in the Appendix. All observations were performed in Small Window mode with the thin filter. Based on the light curves of XDINSs, we select the appropriate time intervals of observation to reduce the influence of background. Spectra are extracted from circular regions (radii are all 600 in physical mode), and backgrounds are taken from similar nearby source-free areas with the same radii. The extracted spectra are binned with different counts per bin in each observation. The XDINS spectral analysis is performed with XSPEC 12 (Arnaud 1996), selecting photon energies in the 0.1–1.0 keV range.

The results of photometry measured by the *Hubble Space Telescope* (*HST*) and optical data fitted by blackbodies (Rayleigh–Jeans tail at optical bands) are presented in Kaplan et al. (2011). The bremsstrahlung emission is optically thick at

Table 2
Summary of EPIC-pn Observation for Each XDINS

ObsID	R.A.	Decl.	Start Date	End Date	Duration (s)	Counts
0651470601	$04^h\ 20^m\ 01\overset{s}{.}89$	$-50^d\ 22'\ 48\overset{''}{.}1$	2010 Jul 29 14:20:46	2010 Jul 29 16:16:02	6916	1001
0651470701	$04^h\ 20^m\ 01\overset{s}{.}89$	$-50^d\ 22'\ 48\overset{''}{.}1$	2010 Sep 21 08:40:34	2010 Sep 21 11:32:30	10,316	1165
0651470801	$04^h\ 20^m\ 01\overset{s}{.}89$	$-50^d\ 22'\ 48\overset{''}{.}1$	2010 Oct 02 23:05:56	2010 Oct 03 02:27:53	12,117	1426
0651470901	$04^h\ 20^m\ 01\overset{s}{.}89$	$-50^d\ 22'\ 48\overset{''}{.}1$	2010 Oct 03 19:17:37	2010 Oct 03 23:01:09	13,412	1520
0651471001	$04^h\ 20^m\ 01\overset{s}{.}89$	$-50^d\ 22'\ 48\overset{''}{.}1$	2010 Oct 04 05:12:09	2010 Oct 04 10:00:44	17,315	2020
0651471101	$04^h\ 20^m\ 01\overset{s}{.}89$	$-50^d\ 22'\ 48\overset{''}{.}1$	2010 Oct 06 22:57:00	2010 Oct 07 01:59:02	10,915	1103
0651471201	$04^h\ 20^m\ 01\overset{s}{.}89$	$-50^d\ 22'\ 48\overset{''}{.}1$	2010 Nov 26 09:28:48	2010 Nov 26 11:07:23	5915	626
0651471301	$04^h\ 20^m\ 01\overset{s}{.}89$	$-50^d\ 22'\ 48\overset{''}{.}1$	2011 Jan 13 22:23:20	2011 Jan 14 02:48:32	15,912	2149
0651471401	$04^h\ 20^m\ 01\overset{s}{.}89$	$-50^d\ 22'\ 48\overset{''}{.}1$	2011 Mar 31 20:15:41	2011 Mar 31 23:17:38	10,917	797
0311590101	$07^h\ 20^m\ 24\overset{s}{.}96$	$-31^d\ 25'\ 50\overset{''}{.}2$	2005 Nov 12 22:26:18	2005 Nov 13 09:28:08	39,710	205,842
0400140301	$07^h\ 20^m\ 24\overset{s}{.}96$	$-31^d\ 25'\ 50\overset{''}{.}2$	2006 May 22 04:44:47	2006 May 22 10:49:56	21,909	55,147
0400140401	$07^h\ 20^m\ 24\overset{s}{.}96$	$-31^d\ 25'\ 50\overset{''}{.}2$	2006 Nov 05 11:19:29	2006 Nov 05 17:24:41	21,912	139,743
0502710201	$07^h\ 20^m\ 24\overset{s}{.}96$	$-31^d\ 25'\ 50\overset{''}{.}2$	2007 May 05 17:01:25	2007 May 05 23:06:32	21,907	26,960
0502710301	$07^h\ 20^m\ 24\overset{s}{.}96$	$-31^d\ 25'\ 50\overset{''}{.}2$	2007 Nov 17 05:14:32	2007 Nov 17 12:09:53	24,921	154,377
0552210201	$08^h\ 06^m\ 23\overset{s}{.}40$	$-41^d\ 22'\ 30\overset{''}{.}9$	2008 May 11 10:45:37	2008 May 11 13:17:31	9114	10,681
0552210301	$08^h\ 06^m\ 23\overset{s}{.}40$	$-41^d\ 22'\ 30\overset{''}{.}9$	2008 May 15 05:59:36	2008 May 15 08:49:49	10,213	11,654
0552210401	$08^h\ 06^m\ 23\overset{s}{.}40$	$-41^d\ 22'\ 30\overset{''}{.}9$	2008 May 29 05:46:24	2008 May 29 07:24:57	5913	5170
0552210601	$08^h\ 06^m\ 23\overset{s}{.}40$	$-41^d\ 22'\ 30\overset{''}{.}9$	2008 Oct 15 10:22:41	2008 Oct 15 13:06:16	9815	11,415
0552211001	$08^h\ 06^m\ 23\overset{s}{.}40$	$-41^d\ 22'\ 30\overset{''}{.}9$	2008 Dec 10 09:38:11	2008 Dec 10 12:22:25	9854	11,645
0552211101	$08^h\ 06^m\ 23\overset{s}{.}40$	$-41^d\ 22'\ 30\overset{''}{.}9$	2009 Mar 31 20:31:05	2009 Mar 31 22:59:43	8918	6828
0552211501	$08^h\ 06^m\ 23\overset{s}{.}40$	$-41^d\ 22'\ 30\overset{''}{.}9$	2008 Nov 09 05:54:53	2008 Nov 09 10:54:07	17,954	1219
0552211601	$08^h\ 06^m\ 23\overset{s}{.}40$	$-41^d\ 22'\ 30\overset{''}{.}9$	2009 Apr 11 00:05:54	2009 Apr 11 02:34:34	8920	3460
0672980201	$08^h\ 06^m\ 23\overset{s}{.}40$	$-41^d\ 22'\ 30\overset{''}{.}9$	2011 May 02 19:47:54	2011 May 02 22:33:10	9916	11,293
0672980301	$08^h\ 06^m\ 23\overset{s}{.}40$	$-41^d\ 22'\ 30\overset{''}{.}9$	2012 Apr 20 07:45:20	2012 Apr 20 09:23:51	5911	6544
0402850301	$13^h\ 08^m\ 48\overset{s}{.}30$	$+21^d\ 27'\ 06\overset{''}{.}8$	2006 Jun 08 22:15:17	2006 Jun 09 00:18:56	7419	4365
0402850401	$13^h\ 08^m\ 48\overset{s}{.}30$	$+21^d\ 27'\ 06\overset{''}{.}8$	2006 Jun 16 21:28:31	2006 Jun 16 23:48:52	8421	15,118
0402850501	$13^h\ 08^m\ 48\overset{s}{.}30$	$+21^d\ 27'\ 06\overset{''}{.}8$	2006 Jun 27 02:33:18	2006 Jun 27 06:01:55	12,517	3692
0402850701	$13^h\ 08^m\ 48\overset{s}{.}30$	$+21^d\ 27'\ 06\overset{''}{.}8$	2006 Dec 27 14:39:39	2006 Dec 27 17:33:10	10,411	19,898
0402851001	$13^h\ 08^m\ 48\overset{s}{.}30$	$+21^d\ 27'\ 06\overset{''}{.}8$	2007 Jun 11 13:52:19	2007 Jun 11 16:54:19	10,920	21,144
0302140101	$16^h\ 05^m\ 18\overset{s}{.}52$	$+32^d\ 49'\ 18\overset{''}{.}0$	2006 Feb 08 00:46:03	2006 Feb 08 05:07:27	15,684	34,312
0302140401	$16^h\ 05^m\ 18\overset{s}{.}52$	$+32^d\ 49'\ 18\overset{''}{.}0$	2006 Feb 10 00:48:25	2006 Feb 10 05:33:40	17,115	30,622
0302140501	$16^h\ 05^m\ 18\overset{s}{.}52$	$+32^d\ 49'\ 18\overset{''}{.}0$	2006 Feb 12 00:35:22	2006 Feb 12 05:21:17	17,155	9660
0302140901	$16^h05^m\ 18\overset{s}{.}52$	$+32^d\ 49'\ 18\overset{''}{.}0$	2006 Feb 16 00:16:37	2006 Feb 16 05:01:51	17,114	38,481
0165972101	$18^h\ 56^m\ 35\overset{s}{.}41$	$-37^d\ 54'\ 34\overset{''}{.}0$	2006 Mar 26 15:34:31	2006 Mar 27 11:01:17	70,006	350,570
0412600301	$18^h\ 56^m\ 35\overset{s}{.}41$	$-37^d\ 54'\ 34\overset{''}{.}0$	2007 Oct 04 05:42:44	2007 Oct 05 01:15:26	70,362	110,060
0412600701	$18^h\ 56^m\ 35\overset{s}{.}41$	$-37^d\ 54'\ 34\overset{''}{.}0$	2009 Mar 19 21:23:59	2009 Mar 20 16:32:37	68,918	240,880
0412600801	$18^h\ 56^m\ 35\overset{s}{.}41$	$-37^d\ 54'\ 34\overset{''}{.}0$	2009 Oct 07 12:01:04	2009 Oct 08 10:44:41	81,817	31,489
0502040701	$21^h\ 43^m\ 03\overset{s}{.}28$	$+06^d\ 54'\ 17\overset{''}{.}0$	2007 May 17 20:56:55	2007 May 18 00:40:24	13,409	19,883
0502040901	$21^h\ 43^m\ 03\overset{s}{.}28$	$+06^d\ 54'\ 17\overset{''}{.}0$	2007 Jun 12 20:44:12	2007 Jun 12 23:09:27	8715	12,024
0502041001	$21^h\ 43^m\ 03\overset{s}{.}28$	$+06^d\ 54'\ 17\overset{''}{.}0$	2007 Nov 03 09:34:53	2007 Nov 03 12:03:33	8920	13,323
0502041101	$21^h\ 43^m\ 03\overset{s}{.}28$	$+06^d\ 54'\ 17\overset{''}{.}0$	2007 Nov 07 04:16:04	2007 Nov 07 07:29:13	11,589	16,889
0502041201	$21^h\ 43^m\ 03\overset{s}{.}28$	$+06^d\ 54'\ 17\overset{''}{.}0$	2007 Nov 08 03:41:28	2007 Nov 08 06:26:46	9918	14,568
0502041801	$21^h\ 43^m\ 03\overset{s}{.}28$	$+06^d\ 54'\ 17\overset{''}{.}0$	2008 May 19 04:11:47	2008 May 19 06:27:05	8118	11,779

optical/UV bands, so the value of $T_e(R_{km}^{\infty}/d_{10})^2$ can be determined by these optical/UV data. From Equation (16), we can see that n_{i0} and kT_i are degenerated. We command a parameter $y = n_{i0}^2 kT_i$ to reduce the complexity of the expression. The column density of hydrogen N_H, kT_e, and y are treated as free parameters common to all spectra. The parameter "norm" is $(R/d)^2$, and the value of d is borrowed from Kaplan & van Kerkwijk (2009) in our fitting. To demonstrate the optical/UV excess, we plot a blackbody radiation curve (in the left panel of Figures 1–7) and extrapolate it to optical/UV bands to compare with the bremsstrahlung curve of each XDINS.

The best modeled values and errors of parameters are shown in Table 1. With these parameters, the bremsstrahlung curve and spectral data of each XDINS are reproduced and plotted in Figures 1–7.

4. Discussion

It is worth noting that a strangeon star atmosphere could simply be regarded as the upper layer of a normal NS atmosphere, but with an almost homogeneous electron (or ion) temperature. Therefore, in the strangeon star atmosphere, thermal X-rays from the lower layer of a normal NS atmosphere are prohibited, and relatively more optical/UV photons are then radiated. A hard X-ray cutoff (i.e., without a hard tail) would also be natural in our model.

4.1. Strangeon Star's Plasma Atmosphere

In Section 2.1, we present that a strangeness barrier hinders the ISM-accreted matter permeation, and then this matter forms a two-temperature ($kT_i > kT_e$) plasma atmosphere. It is shown that in Table 1, $y = n_{i0}^2 kT_i \sim 10^{42}\,\mathrm{cm}^{-6}$ keV and $kT_e \sim 100$ eV.

Because $kT_e < kT_i \ll 100\,\mathrm{MeV}$, we can obtain $10^{18}\,\mathrm{cm}^{-3} \ll n_{i0} \lesssim 10^{21}\,\mathrm{cm}^{-3}$ and $10^{-5}\,\mathrm{g\,cm}^{-3} \ll \rho_{i0} \lesssim 10^{-2}\,\mathrm{g\,cm}^{-3}$, where ρ_{i0} is the mass density of ions in the bottom of atmosphere. Then the total mass of the atmosphere is $\sim 10^{-23}$–$10^{-17}\,M_\odot$. However, in a strange quark star model, Usov (1997) presented an estimate for the total atmospheric mass of $\sim 10^{-23}$–$10^{-22}\,M_\odot$, which is consistent with our results. This total mass is much less than the conventional crust mass of $\sim 10^{-5}\,M_\odot$ of a strange quark star (Alcock et al. 1986); hence, the scale is negligible compared to the radius of the star.

In our calculation, it is assumed that the plasma atmosphere formed by the ISM-accreted matter is spherically symmetric. In fact, falling atoms move along the magnetic field lines to the polar cap, and collisions between the ions and electrons could make them diffuse across the magnetic field lines. The ISM-accreted matter diffuses from the polar cap to other parts of the surface effectively, so the plasma atmosphere could be considered as approximately spherically symmetrical on the surface. This progress can be described as a 2D random walk approximately,

$$\frac{R^2}{\tau_{\mathrm{diff}}} \simeq \frac{r_L^2}{\tau_{\mathrm{ie}}}, \tag{17}$$

where τ_{diff} is the timescale of the diffusion, r_L is the Larmor radius, and τ_{ie} is the timescale of the collision between ions and electrons in plasma. In the case of $\tau_{\mathrm{diff}} < \tau_X$, the accreted ions could diffuse effectively, which may imply a weak magnetic field ($\lesssim 10^{10}$ G). This weak magnetic field exhibits a small Alfvén radius, $R_A < R_B$, and then an accretion disk would form. Note that these NSs could be the first observed examples of NSs in the propeller phase (see Alpar 2001). The propeller torque of a fallback disk may modify the period derivative, which makes the characteristic dipole magnetic field much stronger than the real field (e.g., Liu et al. 2014). Also, the phenomenon that XDINSs are radio quiet and thermal in X-ray band (i.e., being "dead" pulsars) could be associated with the fact of a weak magnetic field; otherwise, those NSs would be beyond the death line, thus "active" pulsars.

However, there may not be enough time for ions to diffuse from the polar cap to other parts of the surface during their flavor change, and then the distribution of the atmosphere would not be spherically symmetric. In this case, the electron velocity would be axisymmetric, so that both the thermal statistical emission and free–free absorption coefficients would be multiplied by a factor of $\sim\sqrt{3}$. The nonspherical symmetry of the distribution could make the spectrum flatter than the Rayleigh–Jeans one at optical/UV bands, a topic that will be put into focus in a coming paper.

4.2. The Fitted Parameters of XDINSs

In the bremsstrahlung model, the spectral absorption line differs from that in blackbody models (Haberl et al. 2004; van Kerkwijk et al. 2004). The results of data fitting show that the spectra (except J0720) have broad absorption lines in soft X-ray bands. The absorption lines could have originated from hydrocyclotron oscillation (Xu et al. 2012) or electron cyclotron resonance (Bignami et al. 2003; Xu et al. 2003). Besides, atomic transition lines could be possible but weak in the thermal spectrum of a corona/atmosphere above a strangeon star (Xu 2014).

The spectrum of one source, J0720, could have a power-law component that might be the result of weak magnetospheric activity. The time-dependent spectrum (van Kerkwijk & Kaplan 2007) could lead to a fitting result with a large χ^2/dof value.

The fitted radiation radius of J0806 is about 3 km, and self-bound strange star models, either a strange quark star (Haensel 2001) or a strangeon star, could be the solution. This indicates that J0806 could be a low-mass strangeon star candidate.

J1308 has a pulsed fraction of ∼18% (Kaplan & van Kerkwijk 2005), which hints at a nonspherically symmetrical distribution of the plasma atmosphere. This leads to a fitting result with large errors in our bremsstrahlung model. Additionally, the spectrum of J1308 is flat in 0.1–0.2 keV, which may imply that it has a strong neutral hydrogen absorption.

J1856 can be well fitted by a Rayleigh–Jeans curve at optical bands, and this indicates that the magnetic field's impact on the distribution of the plasma atmosphere is extremely small. Then, the purely thermal spectrum (i.e., Rayleigh–Jeans in optical/UV bands and featureless in soft X-ray bands) may imply that J1856 has a magnetic field that is weaker than we expected. In addition, J1856 has the shortest distance among all XDINSs. This may make the influence of the ISM on the radiation very small. With *XMM-Newton* data selected for negligible X-ray background change, the simultaneous fitting results of J1856 exhibit $\chi^2 = 1.17$, while χ^2 is 1.11 for the *blackbodyrad* model in Xspec 12. The reason for the slightly larger χ^2 might be that our model is necessarily improved in the future and the response/calibration of *XMM-Newton* should be rechecked near 0.2 keV. Additionally, the pulse fraction of J1856 is smaller than 1.3% (Haberl 2007), which is at the observed limits. Thus, J1856 would be the best candidate of XDINSs to probe the NS's mass and radius, which is important to constrain the equation of state of matter at supranuclear density.

For J2143, the optical data cannot be fitted by a Rayleigh–Jeans curve adequately at optical bands, even if the photoelectric absorption is included. One possible reason for the flat spectrum could be that the number density of the particles (ions and electrons) in the plasma atmosphere is smaller than we expected, and the particles then diffuse slowly. Also, maybe the distance from J2143 is longer than we expected (i.e., $d > 500$ pc). The long distance of J2143 makes neutral hydrogen's absorption extremely obvious, so that the spectrum seems flat, which is similar to the case of J1308. In addition, the rather large radius that resulted from the longer distance could also lead to slow diffusion of particles. Another possible reason for the flat spectrum of J2143 would be the resonant cyclotron scattering process of electrons (Tong et al. 2011) in the plasma atmosphere.

4.3. X-Ray Polarization of XDINSs

The model presented in this paper could be tested by future X-ray polarimetry, with which one may eventually differentiate compact star models, as already discussed in Lu et al. (2013). When X-rays propagate across the magnetosphere of an NS, there are two independent linear polarization eigenmodes: the ordinary mode (O-mode, the electric field is in the plane of the wavevector and the magnetic field) and the extraordinary mode (E-mode, perpendicular to the plane). For the atmosphere that has a significant temperature gradient, the E-mode photons come from a deeper and hotter place, so that the thermal X-rays are polarized (Gnedin & Sunyaev 1974).

On the one hand, in our bremsstrahlung model, the temperature gradient can be ignored since the density of the

plasma atmosphere is extremely low, which is different from the case of Zavlin et al. (1996). The emission is optically thick at optical/UV bands, resembling a Rayleigh–Jeans regime, and would show negligible polarization with a weak magnetic field ($B \lesssim 10^{10}$ G). Meanwhile, if the magnetic field is weak, the X-ray emission might not be polarized because the velocity distribution of the plasma is isotropic.

On the other hand, in the case of a strong magnetic field ($B \gtrsim 10^{12}$ G), the opacity coefficients of a magnetized NS's thermal plasma are different for O-mode and E-mode, which could make the emission polarized (Pavlov & Zavlin 2000). Recently, a measured optical linear polarization of J1856 presented a polarization degree P.D. $= 16.43\% \pm 5.26\%$ and a polarization position angle P.A. $= 145^{\circ}.39 \pm 9^{\circ}.44$ that hint at the presence of vacuum birefringence with an inferred magnetic field ($B \sim 10^{13}$ G; Mignani et al. 2017). In the radiative atmosphere of a strangeon star, the strong magnetic field would also make the Landau energy levels split, and the velocity distribution of plasma will be discrete in the direction perpendicular to the magnetic field, which is different from the simple 3D Maxwell velocity distribution. In this case, the polarization might be detectable in both optical bands and X-ray bands, but detailed calculations on this problem are necessary. Additionally, the nonuniform distribution of the plasma atmosphere with a strong magnetic field may make the emission polarized and show X-ray pulsation.

These polarization behaviors could be tested by soft X-ray polarimetry, e.g., the Lightweight Asymmetry and Magnetism Probe expected to be operational on China's space station around 2020 (She et al. 2015).

5. Summary

A model of a two-temperature plasma atmosphere on a strangeon star's surface is proposed and established, and the observed emission of XDINSs could be the result of the bremsstrahlung radiation in the atmosphere. All the spectra of seven XDINSs would be well fitted in this bremsstrahlung model, from X-ray to optical/UV bands. The results of data fitting show that the electron temperatures are ~50–250 eV and the radiation radii are ~3–13 km. According to these results, we suggest a low-mass strangeon star candidate, J0806, with $kT_{\rm e} = 195.2 \pm 2.4$ eV and $R_{\rm opt}^{\infty} = 3.5 \pm 0.1$ km.

We are grateful to Dr. Fangjun Lu at the Institute of High Energy Physics for technical data analysis and to Dr. David Kaplan for providing optical data. Comments and suggestions from Dr. Andrey Danilenko are especially acknowledged about the data reduction and the model. This work is supported by the National Natural Science Foundation of China (11673002, U1531243, 11373011 and U153120003) and the Strategic Priority Research Program of CAS (no. XDB23010200). The FAST Fellowship is supported by the Special Funding for Advanced Users, budgeted and administrated by the Center for Astronomical Mega-Science, CAS.

Appendix
Observational Data of XDINSs from *XMM-Newton*

Previously, we fitted the recent observational data of each XDINS. Due to the short exposure time of these observations, the χ^2/dof values are not as good as in Table 1, but the spectra exhibit similarity, presented in Figures 1–7.

In order to improve the accuracy of data fitting, we try to fit all observed data of each XDINS. The data are performed in small window mode in EPIC-pn simultaneously with multiple observations. A lot of data for J1856 are collected to analyze its spectral evolution with a timescale of ~10 yr (e.g., Sartore et al. 2012). The results of each observation show some differences that may be attributed to changes of positions or accretion rates during the long exposure time. Thus, the data about the same positions on the detector, as well as other sources, are extracted to fit simultaneously, and then we ignore the observations that show some flare. Also, the relation between the temperature and the position of the source centroid on the detector (RAWX and RAWY coordinates; Sartore et al. 2012) in the blackbody model is different from that in the bremsstrahlung. And it is worth noting that J0720 shows a spectrum change (van Kerkwijk et al. 2007), so we extracted the observation data before 2008. Some detailed information for each observation is shown in Table 2. We fit the data for each observation simultaneously, treating $N_{\rm H}$, $T_{\rm e}$, and y as free parameters.

References

Alcock, C., Farhi, E., & Olinto, A. 1986, ApJ, 310, 261
Alpar, M. A. 2001, ApJ, 554, 1245
Arnaud, K. A. 1996, adass V, 101, 17
Bignami, G. F., Caraveo, P. A., De Luca, A., & Mereghetti, S. 2003, Natur, 423, 725
Bondi, H. 1952, MNRAS, 112, 195
Burwitz, V., Haberl, F., Neuhäuser, R., et al. 2003, A&A, 399, 1109
Burwitz, V., Zavlin, V. E., Neuhäuser, R., et al. 2001, A&A, 379, L35
Dai, S., Li, L. X., & Xu, R. X. 2010, SCPMA, 54, 1541
Drake, J. J., et al. 2002, ApJ, 572, 996
Gnedin, Yu. N., & Sunyaev, R. A. 1974, A&A, 36, 379
Haberl, F. 2007, Ap&SS, 308, 181
Haberl, F., Zavlin, V. E., Trüemper, J., & Burwitz, V. 2004, A&A, 419, 1077
Haensel, P. 2001, A&A, 380, 186
Kaplan, D. L., Kamble, A., van Kerkwijk, M. H., & Ho, W. C. G. 2011, ApJ, 736, 117
Kaplan, D. L., & van Kerkwijk, M. H. 2005, ApJL, 635, L65
Kaplan, D. L., & van Kerkwijk, M. H. 2009, ApJ, 705, 798
Kaplan, D. L., van Kerkwijk, M. H., Marshall, H. L., et al. 2003, ApJ, 590, 1008
Lai, D. 2001, RvMP, 73, 629
Lai, X. Y., & Xu, R. X. 2009, MNRAS, 398, L31
Li, Z. S., Qu, Z. J., Chen, L., et al. 2015, ApJ, 798, 56
Liu, X. W., Xu, R. X., Qiao, G. J., Han, J. L., & Tong, H. 2014, RAA, 14, 85
Lu, J. G., Xu, R. X., & Feng, H. 2013, ChPhL, 30, 059501
Mignani, R. P., Testa, V., González Caniulef, D., et al. 2017, MNRAS, 465, 492
Pavlov, G. G., & Zavlin, V. E. 2000, ApJ, 529, 1011
Read, A. M., Sembay, S. F., Abbey, T. F., & Turner, M. J. L. 2006, in Proceedings of The X-ray Universe 2005, ed. A. Wilson (Madrid: European Space Agency), 925
Rybicki, G. B., & Lightman, A. P. 1979, Radiative Processes in Astrophysics (New York: Wiley-Interscience), 393
Sartore, N., Tiengo, A., Mereghetti, S., et al. 2012, A&A, 541, 66
She, R., Feng, H., Muleri, F., et al. 2015, Proc. SPIE, 9601, 96010I
Tong, H. 2016, SCPMA, 59, 1
Tong, H., Xu, R. X., & Song, L. M. 2011, RAA, 11, 1371
Toropina, O. D., Romanova, M. M., Toropin, Yu. M., & Lovelace, R. V. E. 2001, ApJ, 561, 964
Treves, A., Turolla, R., Zane, S., & Colpi, M. 2000, PASP, 112, 297
Trümper, J. E., Burwit, V., Haberl, F., & Zavlin, V. E. 2004, NuPhS, 132, 560
Turolla, R., Zane, S., & Drake, J. J. 2004, ApJ, 603, 265
Usov, V. V. 1997, ApJL, 481, L107
van Driel, A. F., Allan, G., Delerue, C., et al. 2005, PhRvL, 95, 236804
van Kerkwijk, M. H., & Kaplan, D. L. 2007, Ap&SS, 308, 191
van Kerkwijk, M. H., Kaplan, D. L., Durant, M., Kulkarni, S. R., & Paerels, F. 2004, ApJ, 608, 432

van Kerkwijk, M. H., Kaplan, D. L., Pavlov, G. G., & Mori, K. 2007, ApJL, 659, L149
Voges, W., et al. 1996, IAUC, 6420, 2
Xu, R. X. 2002, ApJL, 570, L65
Xu, R. X. 2003, ApJL, 596, L59
Xu, R. X. 2014, RAA, 14, 617
Xu, R. X., Bastrukov, S. I., Weber, F., Yu, J. W., & Molodtsova, I. V. 2012, PhRvD, 85, 023008
Xu, R. X., & Guo, Y. J. 2017, Centennial of General Relativity: A Celebration (Singapore: World Scientific)
Xu, R. X., Tao, D. J., & Yang, Y. 2006, MNRAS, 373, L85
Xu, R. X., Wang, H. G., & Qiao, G. J. 2003, ChPhL, 20, 314
Zakharov, B. G. 2011, JETP, 112, 63
Zavlin, V. E., Pavlov, G. G., & Shibanov, Y. A. 1996, A&A, 315, 141
Zhou, E. P., Lu, J. G., Tong, H., & Xu, R. X. 2014, MNRAS, 443, 2705